A joint computational and experimental evaluation of $CaMn_2O_4$ polymorphs as cathode materials for Ca ion batteries

M. Elena Arroyo-de Dompablo[1,*], Christopher Krich[2], Jessica Nava-Avendaño[3], Neven Biškup[4], M.Rosa Palacín[3] and Fanny Bardé[2]

[1]Malta Consolider Team, Departamento de Química Inorgánica, Universidad Complutense de Madrid, 28040 Madrid, (Spain)

[2] Toyota Motor Europe, Research & Development 3, Advanced Technology 1, Battery team, Technical Centre, Hoge Wei 33 B, B-1930 Zaventem, (Belgium).

[3] Institut de Ciència de Materials de Barcelona (ICMAB-CSIC) Campus UAB, E-08193 Bellaterra, Catalonia (Spain)

[4]Instituto Pluridisciplinar, Universidad Complutense de Madrid, 28040 Madrid, (Spain)

*Corresponding author: e.arroyo@quim.ucm.es

Abstract

The identification of potential cathode materials is a must for the development of a new calcium-ion based battery technology. In this work, we have firstly explored the electrochemical behaviour of marokite-$CaMn_2O_4$ but the experimental attempts to deinsert Ca ion from this compound failed. First principles calculations indicate that in terms of voltage and capacity, marokite-$CaMn_2O_4$ could sustain reversible Ca deinsertion reactions; half decalciation is predicted at an average voltage of 3.7 V with a volume variation of 6%. However, the calculated barriers for Ca diffusion are too high (1 eV), in agreement with the observed difficulty to deinsert Ca ion from the marokite structure. We have extended the computational investigation to two other $CaMn_2O_4$ polymorphs, the spinel and the $CaFe_2O_4$ structural types. Full Ca extraction from these $CaMn_2O_4$ polymorphs is predicted at an average voltage of 3.1 V, but with

a large volume variation of around 20%. Structural factors limiting Ca diffusion in the three polymorphs are discussed and confronted with a previous computational investigation of the virtual-spinel $[Ca]_T[Mn_2]_OO_4$. Regardless the potential interest of $[Ca]_T[Mn_2]_OO_4$ as cathode for Ca ion batteries, calculations suggests that the synthesis of this compound would hardly be feasible. The present results unravel the bottlenecks associated to the design of feasible intercalation Ca electrode materials, and allow proposing guidelines for future research.

Introduction

Secondary (i.e. rechargeable) batteries are a power source widely used in portable devices (such as personal computers, camcorders and cellular phones) and are also increasingly present in transport and stationary applications. While the current state-of-the-art technology is Li-ion, research efforts are intensified towards the development of alternative technologies to satisfy the ever increasing demands for enhanced energy density[1]. Indeed, the use of lithium metal anodes with high electrochemical capacities (3860 mAh/g) is only possible under certain specific conditions to avoid safety issues and the most used negative electrode material is graphite (372 mAh/g). Efforts to develop successful magnesium anodes (2210 mAh/g) have culminated in proof of concept of this technology. Yet, the high charge-to-radius ratio for magnesium ions has resulted only in very covalent hosts such as $Mo_6S_{8-y}Se_y$ (y=1,2) Chevrel phases fulfilling the requirements to be used as cathode materials. [2] We have recently reported on the feasibility and reversibility of calcium plating in conventional alkyl carbonate electrolytes at moderate temperatures [3] which opens the way to the development of a new rechargeable battery technology using calcium anodes. This is especially attractive given the abundance of calcium on the earth crust[4], the high capacity of calcium anodes (1340 mAh/g), its negative reduction potential (only 170 mV above that of lithium metal) and the lower charge to radius ratio for calcium ions which holds promise of better kinetics when compared to the magnesium based technology. Yet, the identification of potential cathode materials is a must for the new calcium-ion based battery technology. Aside some scattered experimental reports [5-

[8], the screening of potential cathodes was hampered by the lack of suitable electrolytes enabling calcium deposition and stripping.

First principles calculations are a unique tool to accelerate the identification of materials which could sustain reversible intercalation reactions delivering high specific energy [9-13]. A recent computational investigation of spinel AM_2O_4 (M=Ti, V, Cr, Mn, Fe, Co, Ni) revealed the virtual $[Ca]_T[Mn_2]_OO_4$ spinel (T stands for tetrahedral and O for octahedral sites) compound as a potential electrode material for Ca ion batteries [14]. **Figure 1** shows the crystal structure of the virtual $[Ca]_T[Mn_2]_OO_4$ spinel, hereafter denoted as SP. To the best of our knowledge, this compound has not been prepared to date, which might be related to the difficulty of placing Ca ions in Tetrahedral (T) sites. In the nature, the composition $CaMn_2O_4$ forms the marokite mineral [15], whose structure is commonly denoted post-spinel structural type and hereafter denoted as CM. This comes from the well-known transformation under pressure of some spinel-like compounds to the $CaMn_2O_4$ marokite-structure [16-19]. The structure of post-spinel (or marokite) $CaMn_2O_4$ (Space Group, S.G. *Pbcm*) is built up from edge-sharing chains of MnO_6 octahedra, forming double rutile chains. Each double-rutile chain is connected to two adjacent chains through edge-sharing oxygen and another two chains through corner-sharing oxygen. As a result, tunnels appear in the framework, where Ca ion can reside in eight-fold coordination (see **figure 1**). The MnO_6 octahedra in the structure are distorted by the Jahn-Teller effect of octahedral Mn^{3+} in high spin configuration. Under high pressure treatment, marokite transforms to another post-spinel structural type [16], the $CaFe_2O_4$ type (S.G. *Pnma*), which shows a very similar structure, but with the double-rutile chains interconnected only through vertex sharing oxygen. Note that the S.G. given in the literature for post-spinel structures changes with the different axis settings. In this work we will refer to the crystal structures of $CaMn_2O_4$ and $CaFe_2O_4$ as CM and CF, respectively.

Post-spinel phases AMn_2O_4 (A = Li, Na, Mg) have been investigated as positive electrode materials in rechargeable batteries. Ling et al. reported a low energy barrier for the diffusion of A ions along the tunnel in the post spinel structures, making the virtual compound

$MgMn_2O_4$ very appealing as cathode for Mg ion batteries [20]. The synthesis of AMn_2O_4 (A = Li, Na, Mg) requires the high pressure treatment of the respective spinel phases; $LiMn_2O_4$ can be prepared at 6 GPa [21] and $NaMn_2O_4$ at 4.5 GPa [22]. The as-prepared $NaMn_2O_4$ displays a capacity retention of 60 mAh/g with cycling at an average voltage of 3V vs. Na^+/Na [22]. Given the interest of post-spinel materials as intercalation electrodes for Li, Na and Mg ion batteries, the marokite-$CaMn_2O_4$ appears as a prior candidate to initiate the quest for cathode materials for Ca ion batteries. In this work, we explore the electrochemical behaviour of marokite-$CaMn_2O_4$ (CM polymorph) through a combined experimental and computational approach. While experimentally the investigation of the SP and CF-$CaMn_2O_4$ polymorphs is, at the moment, impracticable, a computational exploration of the three polymorphs (CM, CF and SP) provides a more general understanding of the properties-structure relationships. Elucidating such trends is of paramount importance as they should serve as guidelines in the development of materials that exhibit reversible Ca ion intercalation, which has been to date an insurmountable challenge for solid state chemists. In this context, the present DFT investigation serves to gain broader insights to advance the search for Ca cathode materials

Methodology

Experimental.- We have prepared $CaMn_2O_4$ by a solid state route [23] . A mixture of MnO_2 and $CaCO_3$ reactants was ground and pelletized. Two heat treatments of 72 hours at 1200°C with a grinding and re-pelletizing in between were necessary to achieve an appropriate purity. Rietveld refinement on the ground pellet revealed $CaMn_2O_4$ in the marokite phase to be present at 99.89%. The impurity phase is MnO.

Coated electrodes are produced by mixing the $CaMn_2O_4$ powder with carbon and binder (polyvinylidene fluoride, in short PVDF) in a weight ratio of 80:10:10. N-Methyl-2-Pyrrolidone (NMP) is added until a slurry forms presenting adequate viscosity. The slurry is coated on aluminum foil with a blade gap of 350 μm. Subsequently, the foil is placed in a vacuum oven for drying at 80 ºC for 24 hours. Three electrode Swagelok cells were used for all

measurements. Calcium metal was used as counter and Lithium metal as reference electrodes, respectively. Electrochemical tests were done at temperatures between 50 ºC and 75 ºC in order to allow effective calcium plating/stripping at the counter electrode [3]. 0.4M solution of $Ca(BF_4)_2$ in EC:PC (1:1 in volume) was used as electrolyte. The water content in the electrolyte was estimated by Karl Fischer titration technique to be below 110 ppm. Electrochemical tests were done under different galvanostatic and potentiostatic protocols on a VMP3 potentiostat (Bio-Logic). XRD patterns were taken on a Rigaku MiniFlexII Diffractometer for both pristine and electrochemically tested samples. For the latter an air-tight dome sample holder with a Kapton foil window was used.

Computational.- The calculations have been performed using the ab-initio total-energy and molecular dynamics program VASP (Vienna ab-initio simulation program) developed at the Universität Wien [24]. For the CM and CF polymorphs, total energy calculations based on Density Functional Theory (DFT) were performed within the General Gradient Approximation (GGA), with the exchange and correlation functional form developed by Perdew, Burke, and Ernzerhof (PBE). [25] The interaction of core electrons with the nuclei is described by the Projector Augmented Wave (PAW) method.[26] We have also calculated the total energy of SP, CM and CF- $CaMn_2O_4$ and Mn_2O_4 within the GGA+U method, following the simplified rotationally invariant form of Dudarev, et al.[27], using U and J values of 5 eV and 1 eV, respectively, for the *d* orbitals of Mn ions (*Ueff= 4* eV). The energy cut off for the plane wave basis fixed at a constant value of 600 eV throughout the calculations. The integration in the Brillouin zone is done on an appropriate set of *k*-points determined by the Monkhorts-Pack scheme. A convergence of the total energy close to 10 meV per formula unit is achieved with such parameters. A ferromagnetic configuration was selected in all cases. All crystal structures were fully relaxed (atomic positions, cell parameters and volume). The final energies of the optimized geometries were recalculated to correct the changes in the basis set of wave functions during relaxation.

For the three $CaMn_2O_4$ polymorphs (CM, CF and SP), the unit cell utilized in the calculation comprises 4 formula units ($Ca_4Mn_8O_{16}$). The initial positions for the CM, CF and SP polymorphs were taken from marokite [28], $CaFe_2O_4$ [29] and $CdMn_2O_4$ [30], respectively. The crystal models for the deinserted Mn_2O_4 were constructed removing all the Ca ions from the fully relaxed structures of the respective polymorph (SP, CM and CF-$CaMn_2O_4$). To investigate the intermediate $Ca_xMn_2O_4$ phases ($0 < x < 1$) a certain Calcium/vacancy ordering needs to be defined. In the present work ordered Calcium/vacancy configurations were constructed using the CASM software package. [31, 32] We firstly considered possible orderings within the unit cell ($Ca_4Mn_8O_{16}$), where only one configuration $Ca_xMn_2O_4$ is possible for x = 0.25 ($CaMn_8O_{16}$) and x = 0.75 ($Ca_3Mn_8O_{16}$). At half decalciation ($Ca_2Mn_8O_{16}$) up to three Ca/vacancy configurations are possible, since any other Calcium/vacancy configurations are equivalent by symmetry considerations. These $Ca_{0.5}Mn_2O_4$ configurations are shown in the S.I. In order to investigate a larger number of Cacium/vacancy orderings, $Ca_8Mn_{16}O_{32}$ supercells were constructed and the total energy of some $Ca_4Mn_{16}O_{32}$ configurations were computed.

We have investigated calcium mobility in $CaMn_2O_4$ using the Nuged Elastic Band method (NEB) as implemented in VASP. NEB calculations are usually carried out at the dilute limits, that is, either the migration of a single vacancy in an otherwise fully calciated structure or a single calcium migration in an otherwise calcium-free host structure. [33] Large supercells are required to attain the dilute limit, but, since NEB calculations are expensive, the size of the supercell is limited by the computational resources. In the present work, we used $Ca_{16}Mn_{32}O_{64}$ supercells (12 Å x 10 Å x 10 Å), that guarantees a minimum interaction between defects (vacancies). Constant volume calculations were performed for three intermediate images initialized by linear interpolation between the two fully relaxed $Ca_{15}Mn_{32}O_{64}$ end points.

To investigate the thermodynamic stability of $CaMn_2O_4$ polymorphs, starting from the optimized structures of the CM and SP forms, we performed relaxed structure calculations at various constant volumes. The energy (E) as a function of the volume (V) was fitted to a second order Birch-Murnaghan Equation Of State [34, 35] (EOS). By means of the quasi-harmonic Debye

model [36, 37], it is possible to extrapolate the *ab initio* data to finite temperatures and evaluate the thermodynamic properties of the system [38, 39]. Under this approximation, the true phonon spectrum is replaced by a smooth function that depends on a single parameter: the Debye temperature, $\Theta_D(V)$. We have used this approximation to obtain preliminary thermodynamic information of the polymorphic CM→ SP transformation at finite temperature. GIBBS code [40], a thermodynamic package, allows us to automatically process the E(V) data obtained from DFT calculations and investigate the isothermal-isobaric thermodynamics of solids. In this work, thermal effects were computed using the Debye temperature calculated from the static bulk moduli and a Poison ratio of 0.25 was used.

Results

a) Synthesis and Electrochemistry of marokite- The XRD patterns of the synthesized marokite phase are given in **Figure 2a**. Refined lattice parameters are 3.15866Å, 9.99365Å and 9.67475Å, in good agreement with previous works. Small amounts of a MnO phase were detected and were quantified by Rietveld refinement to be around 0.1%. The synthesis produces a relatively large particle size distribution (1μm - 10μm), as can be seen in the SEM image (S.I.).

Figure 2b shows the potential vs. capacity plot of a $CaMn_2O_4$ coated electrode tested by potentiodynamic intermittent titration technique (PITT) by applying a 5mV step and a cut off current of C/200 at 75°C. The oxidation process detected at 4.3 V is indicative of the electrolyte degradation. Note that the current was manually reversed since the oxidation process seems not to come to an end, therefore the capacity reported corresponds to a certain degree electrolyte decomposition which would otherwise last until all the electrolyte would be consumed. The XRD pattern of the electrode recovered after oxidation shows no differences with the pristine sample (see **S.I**.). Similar results are obtained using different C rates and temperatures (50 ºC) and thus there is no evidence of electrochemical activity related to the calcium deinsertion from the active material.

b) DFT investigation of electrode characteristics of $CaMn_2O_4$ polymorphs. The crystal lattice and physical properties of marokite-$CaMn_2O_4$ are well reproduced within both the GGA and GGA+U approximations (see **table I in S.I**.). Both methods agree predicting semiconducting behaviour for $CaMn_2O_4$ (band gap < 1 eV), and metallic for the deinserted marokite. For the three investigated polymorphs the Mn oxidation state is fully consistent with high spin Mn^{3+} ions in $CaMn_2O_4$ and Mn^{4+} ions in Mn_2O_4.

Figure 3 represents the calculated energy and volume differences between the CM, CF and SP structures, for x = 1 and x = 0 (GGA+U results). At x = 1, we found the CM type 0.3 eV more stable that the denser CF, which is consistent with the observed transition of the marokite (CM type) to the CF type under high pressure [16]. At x = 0, the CF type is predicted more stable than the CM type by 1.1 eV. This inversion of relative stability as a function of x seems to be in line with the dependence of the CM / CF relative stability with the cations size evidenced by Ling et al., who found the CF-AMn_2O_4 type more stable for Li and Mg, and the CM-AMn_2O_4 type more stable for the larger Na ion [20]. Interestingly, the SP and the CF types are equally stable at both x=1 (energy difference 0.02/f.u eV) and x=0 (energy difference 0.05 eV/f.u) , an issue discussed below.

Figure 4 shows the calculated average voltage and volume changes associated with the Ca deinsertion reaction:

$$CaMn_2O_4 \rightarrow Ca + Mn_2O_4 \qquad (1)$$

The calculated average voltages of the *full* Ca deinsertion from both SP and CF types are 3.1 V, whilst the thermodynamically stable form, the CM type, presents a higher voltage of 3.8 V. For all structures, the calculated volume contraction for reaction (1) is around 20%, suggesting that reversible extraction/insertion of all Ca ions from $CaMn_2O_4$ may be difficult. This handicap has been also found in a recent DFT investigation of $CaMO_3$ as cathode for Ca batteries, with volume change of 20% for the full Ca deinsertion.[13] Yet, it might be possible to *partially* deinsert Ca from $CaMn_2O_4$ with moderate crystal structure modifications, and at lower voltages, if the formation of intermediate phases $Ca_xMn_2O_4$ ($0 < x < 1$) were thermodynamically

favourable. We have investigated this possibility for the CM type. We defined the formation energy for a given Ca-vacancy distribution with composition x as:

$$\Delta_f E = E - x\, E_{CaMn2O4} - (1-x)\, E_{Mn2O4} \qquad (2)$$

Where E is the total energy of the configuration per CM-$Ca_xMn_2O_4$ formula unit, $E_{CaMn2O4}$ is the energy of the marokite and E_{Mn2O4} is the energy of the CM-deinserted phase. As seen in figure 4a, some $Ca_{0.5}Mn_2O_4$ superstructures have negative formation energies (see S.I. for crystal structures), indicating that partial deinsertion from marokite could be feasible. **Figure 4b** shows the GGA+U calculated voltage composition profile constructed from the convex hull of **figure 4a**; the half deinsertion at 3.7 V has a moderate volume contraction of 6 %. Note that we cannot discard that other $Ca_xMn_2O_4$ ($0 < x \leq 0.5$) configurations may lower formation energies than those studied in the present work. In that case, Ca deinsertion from CM-$CaMn_2O_4$ would occur at voltages below 3.7 V. Values of 3.7 V, or below, fall in the voltage-range of the electrolyte stability. However, we can not exclude that the observed lack of electrochemical activity in the marokite polymorph arises from the existence of a significant overpotential that prevents the observation of calcium deinsertion before electrolyte decomposition takes place. While the overpotential could partially be reduced optimizing the cells components (electrolyte, interfaces, electrode conformation…) it is directly related to the Ca^{2+} diffusivity in the active material.

DFT theory has been applied to investigate the Ca mobility in post spinel $CaMn_2O_4$ (CF and CM types). The most likely path for Ca^{2+} diffusion is along the tunnel built up by interconnected Ca sites (see **figure 1**). As seen in **figure 5a**, the calculated energy barrier for intrachannel Ca diffusion in both CM and CF structures, is above 1 eV, this is to say, too high to expect good Ca mobility. In this tunnel, adjacent Ca sites share a triangular face (**figure 5b**). Therefore, going from one site to the adjacent site, the diffusing Ca ions must pass across this triangular window. At the saddle point, the calculated Ca-O distances in this triangular window are 2.11 Å (CM) and 2.17 Å (CF), indicating that the triangular face is too small to allow Ca mobility (note that r $Ca^{2+}{}_{(VI)}$ = 1.0 Å, r O^{2-} = 1.26 Å). For sake of comparison, we have calculated the Li mobility along the tunnel in CF-$LiMn_2O_4$. In good agreement with Ling et al.

[20] we found a low barrier for Li motion, below 0.15 eV. At the saddle-point, the calculated minimum Li-O distances is of 1.95 Å, which is greater than the sum of the ionic radii (r $Li^{+}_{(IV)}$ = 0.59 Å, r O^{2-} = 1.26 Å). This result supports that Ca^{2+} ions are too large and polarizing (compared to Li^{+}) to diffuse in the tunnel of the post-spinel structures.

Although the discussed movement along the tunnel is the most likely, for sake of completeness we have also calculated the energy barrier for the inter-channel motion. **Figure 5c** shows the path for a Ca ion diffusing from one Ca site to another site in a next tunnel, which is 5.4 Å away. The calculated energy barrier is as high as 4 eV. At the saddle point, the diffusing Ca ion shares an edge with the Mn ions. The calculated Mn-Ca distance is of 2.66 Å, to be compared with the 3.20 Å in the end-point. The strong cationic repulsion means a high penalty in energy, hindering Ca mobility along this path.

Regarding the virtual SP-phase, $[Ca]_T[Mn_2]_OO_4$, the calculated barrier by Persson and co-workers [14] is 0.5 eV. In the spinel structure the Ca ion move from one tetrahedral site to another tetrahedral site across an octahedral site. To exit the tetrahedral site, the mobile Ca ion must migrate through a triangular face, as in the case of the CM and CF polymorphs. Our calculated O-O distances in that triangular face are 3.73 Å x 2 and 3.37 Å (Area = 5.6 $Å^2$) for the SP structure, and 3.22 Å x 2 and 2.77 Å (Area = 4 $Å^2$) for the CM polymorph. The hypothetical $[Ca]_T[Mn_2]_OO_4$ spinel accommodating the large Ca ions would exhibit tetrahedral sites with large faces, which would allow Ca mobility. In the real post-spinel structure Ca ions sit in larger sites, but with smaller triangular faces that in the end preclude Ca diffusion. In this context, Ca ion mobility will be favoured in structures where Ca occupies low coordination polyhedral sites, as tetrahedral in $CaMn_2O_4$ spinel, yet, synthetizing such highly metastable compounds is a challenge, as described below.

c) On the synthesis of Spinel-$CaMn_2O_4$- The virtual SP-$CaMn_2O_4$ belongs to a family of compounds which are isostructural with the mineral hausmannite (Mn_3O_4), characterized by a full replacement of the Mn^{2+} ions on the tetrahedral sites by M^{2+} ions accompanied by large tetragonal distortions [41]. Tetragonal spinel structures are known for a large number of M^{2+} ions

such as Ni, Cu, Zn, Mg or Cd. Among these cations, Cd^{2+} has the larger ionic size, yet, $CdMn_2O_4$ can be easily prepared by a standard solid-state reaction method at 1173 K [42]. Ca^{2+} ions are more voluminous than Cd^{2+} ions ($r_{(VI)}$ Ca^{2+} = 1.0 Å, $r_{(VI)}$ Cd^{2+} = 0.95Å), and a legitimate question is whether Ca ions could be introduced in the tetrahedral sites of an oxide framework. To the best of our knowledge, no compound is known with Ca^{2+} in tetrahedral sites, neither is the anionic radius for Ca^{2+} in tetrahedral coordination reported. It seems appealing to evaluate possible synthesis strategies to prepare the SP-$CaMn_2O_4$, and a first step is to investigate the relative stability of the SP and CM polymorphs. To isolate a single polymorph, the "general rule" to follow is that pressure favours the low volume phases, and temperature the larger volume forms. As indicated in **figure 3**, the CF and SP phases are both about 0.3 eV/ f.u. less stable than the CM phase. The CM polymorph transforms to the denser CF-polymorph at 30 GPa (room temperature) [43, 16]. The SP phase has lower density than the CM phase, thus, it is a potential high temperature polymorph.

Figure 6 shows the calculated total energy as a function of the volume per f.u. for CM (diamonds) and SP (squares), together with the corresponding fit of the DFT data to the Birch-Murnagham equation of state at 0 K (for fitting parameters, see S.I.). Typically, literature teaches us that in systems where the spinel is the thermodynamically stable form at ambient conditions, high pressure treatment induce the transformation SP→ CM phase. However, in the present case, *the denser postspinel-$CaMn_2O4$ (CM) is the thermodynamically stable form at ambient conditions*. Only temperature (and not pressure) could induce the transformation CM→ SP As seen in figure 6, the global energy minimum corresponds to CM, the polymorph stable at ambient conditions. At a volume of ca. 90 A^3 /f.u. the CM polymorph is destabilized in favor of the softer SP polymorph. Such crossover suggests that the SP polymorph could be, in principle, obtained by heating the CM phase. (For sake of comparison, we refer the reader to the discussion available in S.I. on the calculated Energy-Volume curves, and fit to EOS, of two well-known temperature-induced phase transformation; TiO_2-rutile → TiO_2-anatase[44] and β-

Li_3PO_4 → γ-Li_3PO_4[45]). To produce the CM→SP phase transformation, the free-energy variation of the polymorphic transformation should equal zero:

$$\Delta G_{p=0} = G_{SP} - G_{CM} = 0 \quad (3)$$

$$\Delta G_{p=0} = G_{SP} - G_{CM} = (H_{SP} - TS_{SP}) - (H_{CM} - TS_{CM}) = (H_{SP} - H_{CM}) - (TS_{SP} - TS_{CM}) \quad (4)$$

The temperature of the CM→ SP transformation can be estimated from:

$$T = (H_{SP} - H_{CM}) / (S_{SP} - S_{CM}) \quad (5)$$

The CM → SP transformation is highly endothermic ($H_{SP} - H_{CM}$ = 27.2 kJ/mol at room temperature, see **S.I**.). Preliminary calculations suggest that entropy difference, $S_{SP} - S_{CM}$, at room temperature is of the order of 8.10^{-3} kJ/Kmol, (see **S.I.**). Hence, a rough estimation yields that a very large temperature (T > 3000 K) will be required to induce the CM → SP transformation. This makes the synthesis of SP polymorph by quenching the CM-phase, or $CaMn_2O_4$-precursors from high temperature highly improbable. Although the temperature estimated is very large (T > 3000 K) for a fully ordered spinel, it could be substantially lower for spinel structures presenting Ca^{2+} both in tetrahedral and octahedral interstices. However, in these disordered spinels, part of the Mn ions would most likely occupy tetrahedral sites, blocking the paths for Ca diffusion.

The above results discourage the use of solid-state synthesis routes to prepare SP-$[Ca]_T[Mn_2]_OO_4$, and in a wider context, Mn oxides with Ca in tetrahedral sites. Alternatively, soft-chemistry routes are been for long used to prepare metastable phases. It has been recently shown that after a treatment in acidic media to remove lithium from $LiMn_2O_4$, a $[Mn_2]_OO_4$-spinel framework is obtained, where Mg ions can be electrochemically intercalated in the tetrahedral sites. [46] Similarly, this strategy might be successful for the intercalation of Ca ions in the empty $[Mn_2]_OO_4$ matrix , although the driving force of Ca ion to occupy octahedral sites could induce the migration of Mn^{3+} ions to the tetrahedral sites[47], resulting in $[Ca_x]_{T,O}[Mn_2]_{T,O}O_4$ ($0 < x \leq 1$) compounds.

Conclusions

We have combined experiments and first principles calculations to explore the basic electrode characteristics of $CaMn_2O_4$ polymorphs. The results highlight the bottlenecks associated to the design of feasible intercalation Ca electrode materials, therefore allowing to propose guidelines for future research.

For the three polymorphs, full Ca extraction causes a large volume variation of 20%. Not surprisingly, this is similar to our recent prediction for volume change in $CaMO_3$ materials. Excessive volume variation associated to high specific capacities is a general obstacle for suitable Ca-intercalation electrodes. In the present study, we have shown that in the marokite-phase the existence of stable $Ca_{0.5}Mn_2O_4$ phases would reduce the volume variation to 6% with half decalciation at 3.7 V, which is an interesting voltage for a cathode. This result points towards intercalation compounds possessing stable intermediate phases as the most promising to overcome large crystal lattice variations, although at the expense of working below the maximum theoretical specific capacity.

We found that the barriers for Ca diffusion are very much structure dependent. In the post-spinel structure, the large and polarizing Ca^{2+} ions (compared to Li^+) cannot exit the stable 8-fold coordination sites, which possess too small polyhedral faces. On the contrary, in the spinel-like phase, $[Ca]_T[M_2]_OO_4$, Ca ions sit in tetrahedral sites, whose larger polyhedral faces permit Ca movement. This result suggest that Ca mobility is favoured when Ca ion reside in low coordination sites. However, our results prove that the location of Ca ions in low coordination-sites comes at the expense of an energy penalty in phase stability ($\Delta H_{(298\ K)}$ CM$\rightarrow$SP = 27.2 kJ/mol). Further investigations are thus needed to enable the synthesis of metastable manganese oxides with Ca in low coordination sites.

In conclusion, the present DFT investigation serves to gain broader insights to advance in the search for Ca cathode materials. More specifically, our results prove that viable cathodes for calcium based batteries could be developed provided a compromise is found between phase stability and low fold-coordination environment for Ca ions. In view of these results, we believe

that efforts should be addressed to develop Mn-based compounds for Ca-ion batteries, as manganese is one of the most abundant, environmentally friendly and inexpensive transition metals.

Acknowledgments

Authors are grateful to A. Ponrouch and D. Tchitchekova for assistance with the electrochemical tests, to F. Rosciano for advices related to the material synthesis and characterization and to the Toyota Battery Research division at Higashi Fuji (M6) for financial support. M.E. Arroyo and N. Biškup acknowledge access to computational resources from Universidad de Oviedo (MALTA-Consolider cluster) and the Spanish's national high performance computer service (I2 Basque Centre).

Supporting Information

Figure S.1.- SEM images of synthetized $CaMn_2O_4$ powder and Comparison of XRD patterns of the electrodes before and after electrochemical oxidation. **TABLE I.** Calculated lattice parameters (in Å) for the SP, CM and CF $Ca_xMn_2O_4$ (x = 0,1) structures. **Figure S.2**.- Optimized crystal structures of $Ca_{0.5}Mn_2O_4$ configurations. **Figure S.3.** – Calculated Energy-Volume data for the marokite phase fit to the Birch-Murnagham equation of state, fixing B_0´to 4.

References

(1) Muldoon, J.; Bucur, C. B.; Gregory, T. Quest for Nonaqueous Multivalent Secondary Batteries: Magnesium and Beyond. *Chem. Rev.* **2014,** 114, 11683-11720.

(2) Aurbach, D.; Lu, Z.; Schechter, A.; Gofer, Y.; Gizbar, H.; Turgeman, R.; Cohen, Y.; Moshkovich, M.; Levi, E. Prototype systems for rechargeable magnesium batteries. *Nature* **2000,** 407, 724-727.

(3) Ponrouch, A.; Frontera, C.; Barde, F.; Palacin, M. R. Towards a Calcium-based rechargeable battery. *Nat. Mater.* **2015,** DOI:10.1038/NMAT4461.

(4) Turekian, K. K.; Wdedepohl, K. H. Distribution of the elements in some major units of the earth's crust. *Geol. Soc. Am. Bull.* **1961,** 72, 175-192.

(5) Amatucci, G. G.; Badway, F.; Singhal, A.; Beaudoin, B.; Skandan, G.; Bowmer, T.; Plitza, I.; Pereira, N.; Chapman, T.; Jaworski, R. Investigation of yttrium and polyvalent ion intercalation into nanocrystalline vanadium oxide. J. *Electrochem. Soc.* **2001,** 148, A940-A950.

(6) Lipson, A. L.; Pan, B.; Lapidus, S. H.; Liao, C.; Vaughey, J. Y.; Ingram, B. J. Rechargable Ca-ion Batteries; A New Energy Storage System. *Chem. Mater.* **2015,** 27, 8442-8447.

(7) Rogosic, J., *"Towards the Development of Calcium Ion Batteries", PhD thesis* Massachussets Institute of Technology: 2014.

(8) Cabello, M.; Nacimiento, F.; González, J. R.; Ortiz, G.; Alcántara, R.; Lavela, P.; Pérez-Vicente, C.; Tirado, J. L. Advancing towards a veritable calcium-ion battery: CaCo2O4 positive electrode material *Electrochem. Comm.* **2016,** 67, 59-64.

(9) Islam, M. S.; Fisher, C. A. J. 'Lithium and sodium battery cathode materials: computational insights into voltage, diffusion and nanostructural properties '. *J. Chem. Soc. Rev.* **2014,** 43, 185-204.

(10) Ceder, G. Opportunities and challenges for first-principles materials design and applications to Li battery materials. *Mater. Res. Soc. Bull.* **2010,** 35, 693-701.

(11) Meng, Y. S.; Arroyo-de Dompablo, M. E. First principles computational materials desing for energy storage materials in lithium ion batteries. *Energy Environ. Sci.* **2009,** 2, 589-609.

(12) Ponrouch, A.; Tchitchekova, D.; Frontera, C.; Bardé, F.; Arroyo-de Dompablo, M. E.; Palacín, M. R. Assessing Si-based anodes for Ca-ion batteries: Electrochemical decalciation of CaSi2. *Electrochem. Commun.* **2016,** 66, 75-78.

(13) Arroyo-de Dompablo, M. E.; Krich, C.; Nava-Avendaño, J.; Palacín, M. R.; Bardé, F. In quest of cathode materials for Ca ion batteries: the CaMO3 perovskites (M = Mo, Cr, Mn, Fe, Co, Ni) *Phys. Chem. Chem. Phys.* **2016,** DOI: 10.1039/C6CP03381D

(14) Liu, M.; Rong, Z.; Malik, R.; Canepa, P.; Jain, A.; Ceder, G.; Persson, K. A. Spinel compounds as multivalent battery cathodes: a systematic evaluation based on ab initio calculations. *Energy Environ. Sci.* **2015,** 8, 964-974.

(15) Gaudefroy, C.; Jouravsky, G.; Permingeat, F. La marokite, CaMn2O4, une nouvelle esp`ece min´erale. *Bull. Soc. Fr. Mineral Crystallogr.* **1963,** 86, 359-367.

(16) Yamanaka, T.; Uchida, A.; Nakamoto, Y. Structural transition of post-spinel phases CaMn2O4, CaFe2O4, and CaTi2O4 under high pressures up to 80 GPa. *Am. Mineral.* **2008,** 93, 1874-1881.

(17) Ito, E.; Takahashi, E. Postspinel transformations in the system Mg2SiO4-Fe2SiO4 and some geophysical implications. *J. Geophys. Res.* **1989**, 94, 10637-10646.

(18) Ono, S.; Kikegawa, T.; Ohishi, Y. The stability and compressibility of MgAl2O4 high-pressure polymorphs. *Phys. Chem. Miner.* **2006,** 33, 200-206.

(19) Errandonea, D., In *Pressure-Induced Phase Transitions in AB2X4 Chalcogenide Compounds*, Springer Berlin Heidelberg: Vol. 189.

(20) Ling, C.; Mizuno, F. Phase Stability of Post-spinel Compound AMn(2)O(4) (A = Li, Na, or Mg) and Its Application as a Rechargeable Battery Cathode. *Chem. Mater.* **25**, 3062-3071.

(21) Yamaura, K.; Huang, Q.; Zhang, L.; Takada, K.; Baba, Y.; Nagai, T.; Matsui, Y.; Kosuda, K.; Takayama-Muromachi, E. Spinel-to-CaFe2O4-type structural transformation in LiMn2O4 under high pressure. *J. Am. Chem. Soc.* **2006,** 128, 9448-56.

(22) Liu, X.; Wang, X.; Iyo, A.; Yu, H.; Li, D.; Zhou, H. High stable post-spinel NaMn2O4 cathode of sodium ion battery. *J. Mater. Chem. A* **2014,** 2, 14822-14826.

(23) Zouari, S.; Ranno, L.; Cheikh-Rouhou, A.; Isnard, O.; Pernet, M.; Wolfers, P.; Strobel, P. New model for the magnetic structure of the marokite-type oxide CaMn2O4. *J. Alloys Comp.* **2003,** 353, 5-11.

(24) Kresse, G.; Furthmuller, J. Efficient Iterative Schemes for Ab Initio Total-Energy Calculations Using a Plane-Wave Basis Set. *Phys. Rev. B* **1996,** 54, 11169.

(25) Perdew, J. P.; Burke, K.; Ernzerhof, M. Generalized gradient approximation made simple. *Phys. Rev. Lett.* **1996,** 77, 3865-3868.

(26) Blöch, P. E. Projector augmented-wave method. *Phys. Rev. B* **1994,** 50, 17953.

(27) Dudarev, S. L.; Botton, G. A.; Savrasov, S. Y.; Szotek, Z.; Temmerman, W. M.; Sutton, A. P. Electronic structure and elastic properties of strongly correlated metal oxides from first principles: LSDA+U, SIC-LSDA and EELS study of UO2 and NiO. *Phys. Status Solidi A* **1998,** 166, 429-443.

(28) Ling, C. D.; Neumeier, J. J.; Argyriou, D. N. Observation of antiferromagnetism in marokite CaMn2O4. *J. Solid State Chem.* **2001,** 160, 167-173.

(29) Decker, B. F.; Kasper, J. S. the structure of Calcium ferrite. *Acta Crystallogr.* **1957,** 10, 332-337.

(30) Yinha, A. P. B.; Sanjana, N. R.; Biswas, A. B. The crystal structure of cadmium manganite, Cd(Mn2)O4. *Z.Kristallogr. Kristallgeom. Kristallphys. Kristallchem.* **1957,** 109, 410-421.

(31) Van der Ven, A.; Thomas, J. C.; Qingchuan Xu; Swoboda, B.; Morgan, D. Nondilute diffusion from first principles: Li diffusion in Li x TiS 2 *Phys. Rev. B* **2008,** 78, 104306.

(32) Van der Ven, A.; Thomas, J. C.; Xu, Q.; Swoboda, B.; Bhattacharga, J. Linking the electronic structure of solids to their thermodynamic and kinetic properties. *Math. Comput. Simulat.* **2010,** 80, 1393.

(33) Deng, Z.; Mo, Y.; Ong, S. P. Computational studies of solid-state alkali conduction in rechargeable alkali-ion batteries. *NPG Asia Mater.* **2016,** 8, e254.

(34) Murnaghan, F. D. The Compressibility of Media under Extreme Pressures *Proc. Natl. Acad. Sci. USA* **1944**, 30, 244.

(35) Birch, F. Finite Elastic Strain of Cubic Crystals. **1947,** Phys. Rev. 71, 809.

(36) Zhang, Y.; Ke, X.; Chen, C.; Yang, J.; Kent, P. Thermodynamic properties of PbTe, PbSe, and PbS: First-principles study. *Phys. Rev. B* **2009,** 80, 024304.

(37) Maradudin, A. A.; Montroll, E. W.; Weiss, G. H. Theory of Lattice Dynamics in The Harmonic Approximation. *Academic Press, London (1971).*

(38) Florez, M.; Recio, J. M.; Francisco, E.; Blanco, M. A.; Martin Pendas, A. First-principles study of the rocksalt–cesium chloride relative phase stability in alkali halides. *P. Phys. Rev. B* **2002,** 66, 144112.

(39) Blanco, M. A.; Martin Pendas, A.; Francisco, E.; Recio, J. M.; Franco, R. Thermodynamical properties of solids from microscopic theory: applications to MgF2 and Al2O3. *J. Mol. Struct-TEOCHEM* **1996,** 368, 245-255.

(40) Blanco, M. A.; Francisco, E.; Luaña, V. GIBBS: isothermal-isobaric thermodynamics of solids from energy curves using a quasiharmonic Debye model. *Comput. Phys. Commun.* **2004,** 158, 57-72.

(41) McClure, D. S. The distribution of transition metal cations in spinels. *J. Phys. Chem. Solids* **1957,** 3, 311-317.

(42) Oliveira, G. N. P.; Teixeira, R.; Mendonca, T. M.; Silva, M. R.; Correia, J. G.; Lopes, A. M. L.; Araujo, J. P. Local symmetry lowering in CdMn2O4 spinel. *J. Appl. Phys.* **2014,** 116.

(43) Wang, Z. W.; Saxena, S. K.; Neumeier, J. J. Raman scattering study on pressure-induced phase transformation of marokite (CaMn2O4). *J. Solid State Chem.* **2003,** 170, 382-389.

(44) Arroyo-de Dompablo, M. E.; Morales-Garcia, A.; Taravillo, M. DFT plus U calculations of crystal lattice, electronic structure, and phase stability under pressure of TiO2 polymorphs. *J. Chem. Phys.* **2011,** 135, 054503.

(45) Arroyo-deDompablo, M. E.; Dominko, R.; Gallardo-Amores, J. M.; Dupont, L.; Mali, G.; Ehrenberg, H.; Jamnik, J.; Moran, E. On the energetic stability and electrochemistry of Li2MnSiO4 polymorphs. *Chem. Mater.* **2008,** 20, 5574-5584.

(46) Kim, C.; Phillips, P. J.; Key, B.; Yi, T.; Nordlund, D.; Yu, Y. S.; Bayliss, R. D.; Han, S. D.; He, M.; Zhang, Z.; Burrell, A. K.; Klie, R. F.; Cabana, J. Direct Observation of Reversible Magnesium Ion Intercalation into a Spinel Oxide Host. *Adv. Mater.* **2015,** 27, 3377-3384.

(47) Reed, J.; Ceder, G.; Van Der Ven, A. Layered-to-spinel phase transition in LixMnO2. *Electrochem. Solid-State Lett.* **2001,** 4, A78.

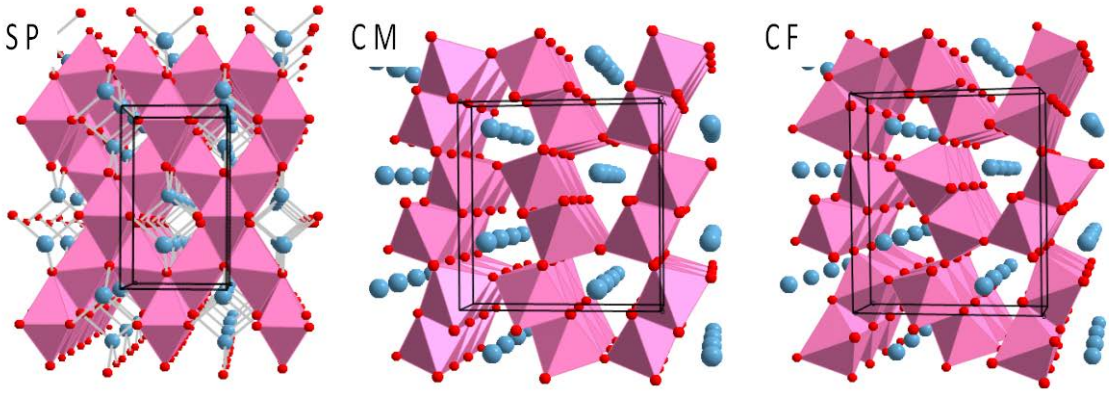

Figure 1- Crystal structures of the investigated $CaMn_2O_4$ polymorphs: the virtual spinel (SP), the post-spinel $CaMn_2O_4$ (CM) and the post-spinel $CaFe_2O_4$-type (CF). Colour code: Ca in blue, Mn in pink, O in red. Note the different connectivity of the double rutile chains in the post-spinel polymorphs.

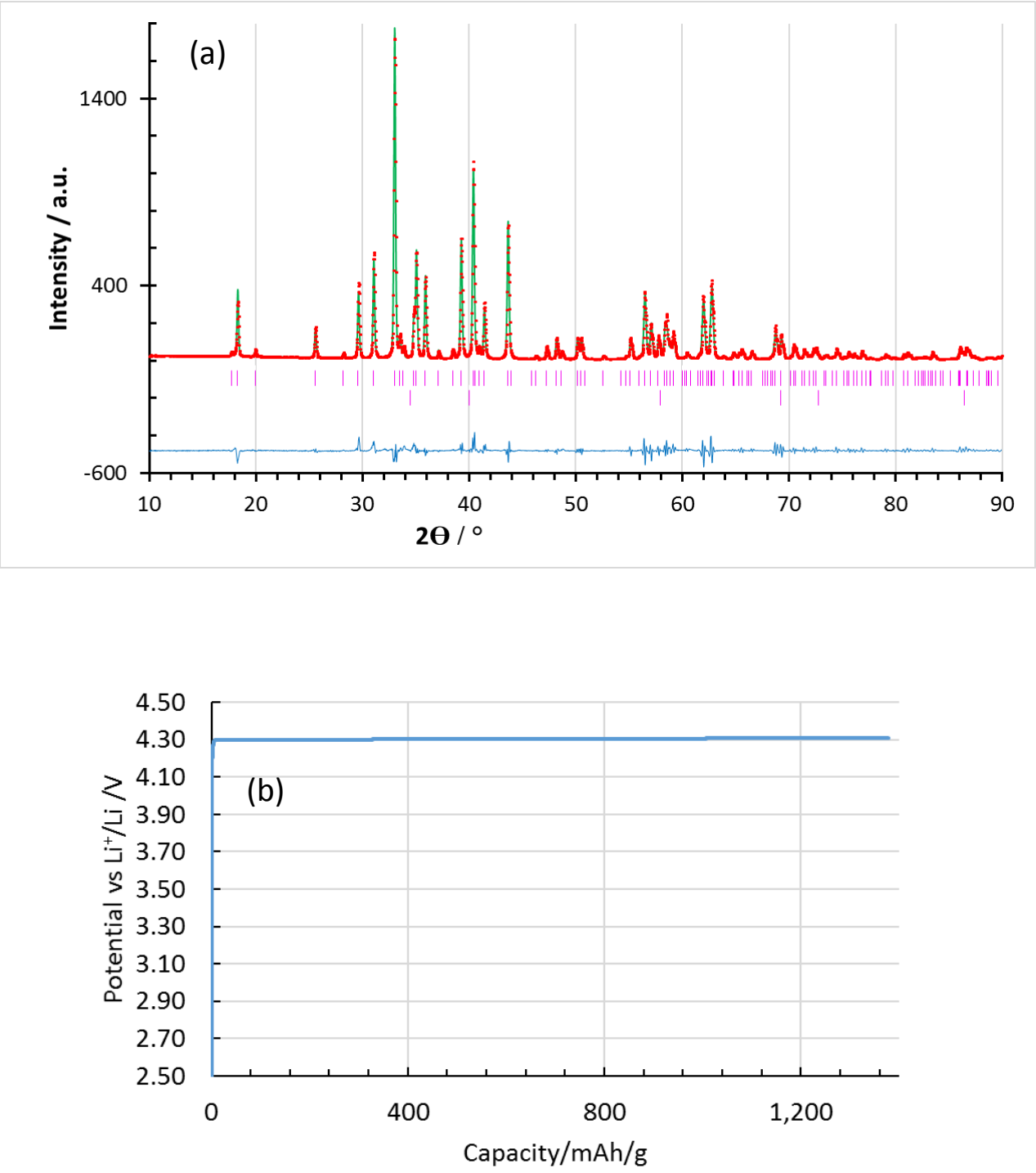

Figure 2- (a) Observed and calculated XRD patterns of as-prepared $CaMn_2O_4$. Red profile is the observed di fferenceogram, blue is the di fference. Vertical b positions of the two phases included in the refinement; $CaMn_2O_4$ (top) and MnO (bottom). (b) Potential vs. capacity profile for $CaMn_2O_4$ tested by PITT with 5mV potential steps and a cut off current of C/200.

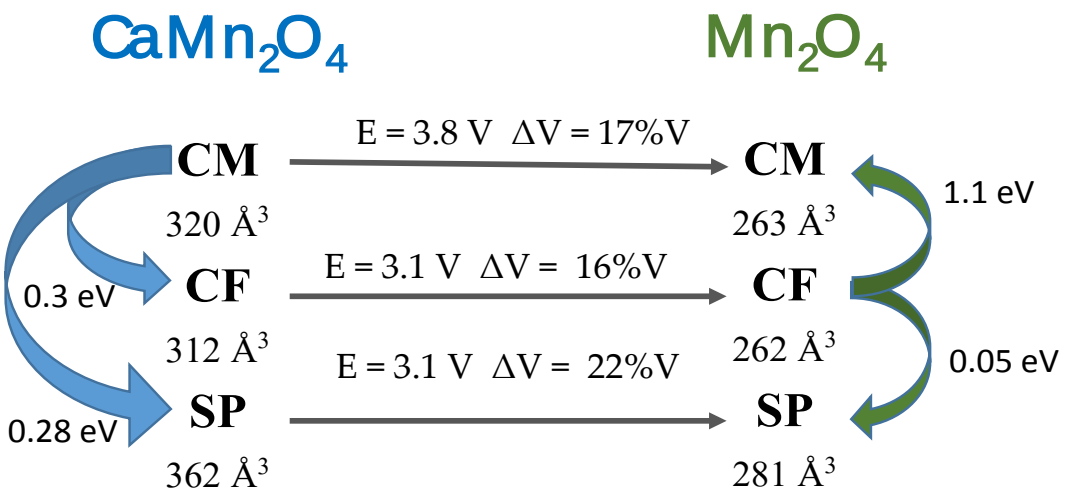

Figure 3- Calculated relative phase stability (eV per formula unit) and volume ($Å^3$ per unit cell) for $Ca_xMn_2O_4$ (x = 0, 1) within the CM, CF and SP crystal structures. Calculated average voltage and volume variation (($VCaMn_2O_4$-VMn_2O_4 *100)/$VCaMn_2O_4$) refer to the reaction $CaMn_2O_4$ → Mn_2O_4 + Ca.

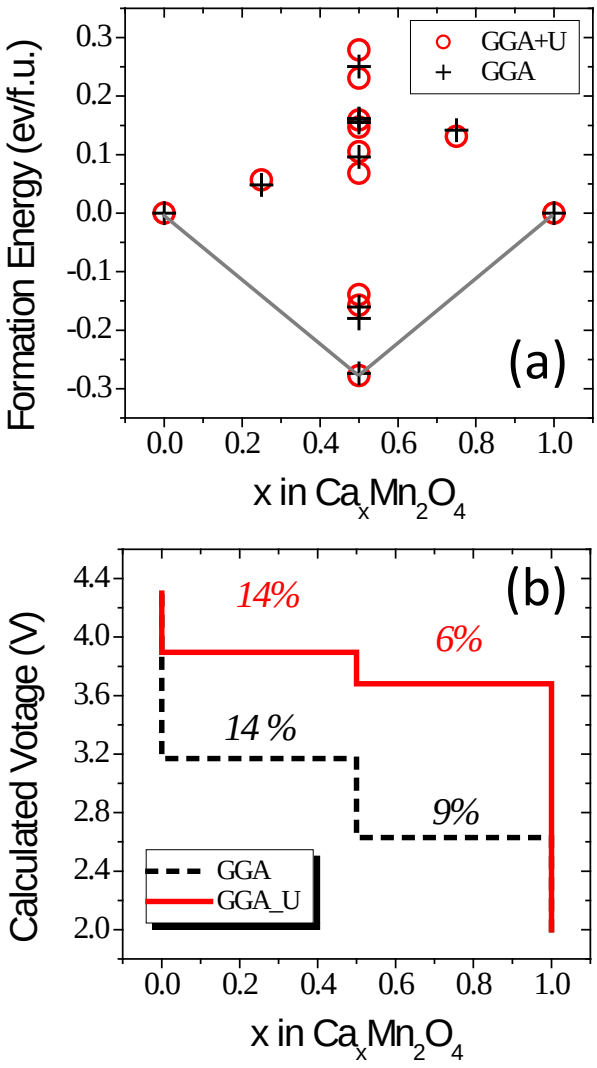

Figure 4- (a) Calculated formation energies of ordered CM-$Ca_xMn_2O_4$ configurations (red circles for GGA+U and black crosses for GGA). (b) Calculated sketch of the voltage – composition curve using the GGA+U with U_{eff} = 4 eV (in red) and GGA (dashed black) approximations. Volume contraction between two consecutive single phases is given as percentage (%).

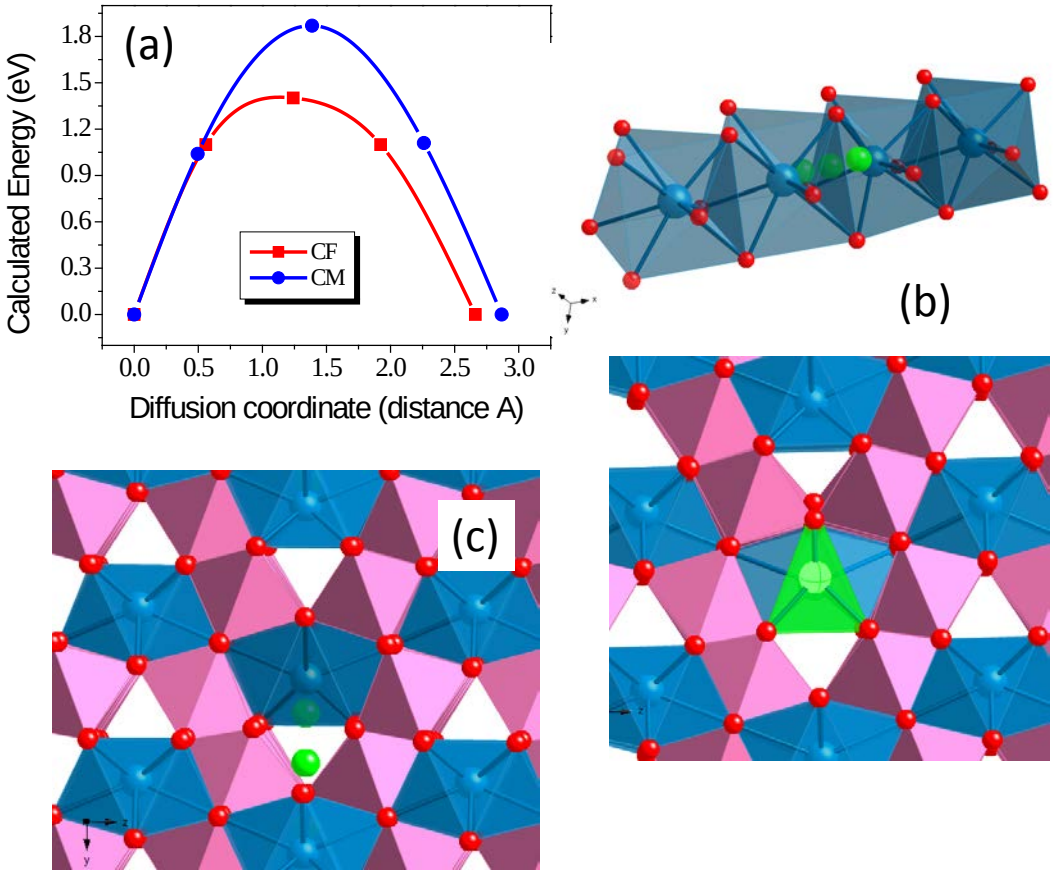

Figure 5.- (a) Calculated energy barriers for intra-channel Ca diffusion in CF-$CaMn_2O_4$ and CM-$CaMn_2O_4$; (b) Views along the *x* axis and in the *yz* plane of the intra-channel Ca diffusion path in the CM structure; (c) View of the path for inter-channel Ca diffusion in the CM structure

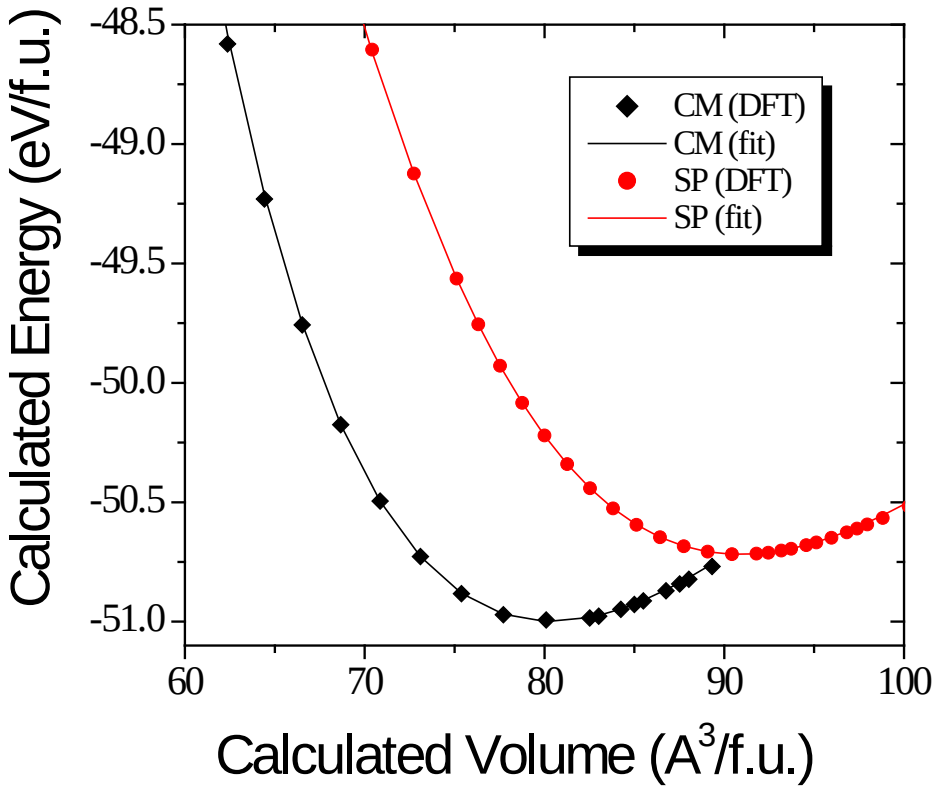

Figure 6. Calculated total energy vs. volume curves of the $CaMn_2O_4$ polymorphs; spinel (SP in red circles) and marokite (CM in black diamonds). Symbols correspond to the DFT calculated data, and lines show the fitting to the Birch-Murnagham equation of state.